CHOICE OF VELOCITY VARIABLES FOR COMPLEX FLOW COMPUTATION

W. Shyy
Department of Aerospace Engineering, Mechanics and Engineering Science
University of Florida, Gainesville, Florida 32611-2031

G. C. Chang
Chung Shan Institute of Science and Technology, Taiwan, ROC

ABSTRACT

The issue of adopting the velocity components as dependent velocity variables for the Navier-Stokes flow computations is investigated. The viewpoint advocated here is that a numerical algorithm should preferably honor both the physical conservation law in differential form and the geometric conservation law in discrete form. With the use of Cartesian velocity vector, the momentum equations in curvilinear coordinates can retain the full conservation-law form and satisfy the physical conservation laws. With the curvilinear velocity components, source terms appear in differential equations and hence the full conservation law form can not be retained. In discrete expressions, algorithms based on the Cartesian components can satisfy the geometric conservation-law form for convection terms but not for viscous terms; those based on the curvilinear components, on the other hand, cannot satisfy the geometric conservation-law form for either convection or viscous terms. Several flow solutions for domain with ninety-degree and three-hundred-sixty-degree turnings are presented to illustrate the issues of using the Cartesian velocity components and the staggered grid arrangement.

INTRODUCTION

Numerical methods for solving the Navier-Stokes flow have been under intensive development for sometime. As is well known, the fundamental issues encountered in the numerical computation arise from many sources, including the construction of appropriate discrete operators for various mechanisms, especially convection terms, the manner of grid distribution, the method of solution procedure of large number of linearized equations, the treatment of the numerical boundary conditions, and the handling of coupling among the dependent variables [1,2]. The present work attempts to investigate a related fundamental question relevant to computing complex fluid flows arising from propulsion components, namely the "suitability" of choosing a specific type of velocity variables as the primary dependent variables of the governing equations [3].

With regard to the choice of the velocity variables, in gross terms, one has the options of using the Cartesian, contravariant, or covariant components as the primary variables. Although comments have been made regarding the suitability of each of these choices [4-6], they are mostly speculations. A more detailed and systematic study is desirable, as is attempted here.

First the relationship between the Cartesian (u, v) and contravariant (U, V) velocity components are defined as follows:

$$U = y_\eta u - x_\eta v \tag{1}$$

$$V = -y_\xi u + x_\xi v \tag{2}$$

Then the continuity equation in ξ- and η-coordinates can be written in the similar form with the contravariant velocity components to that in x- and y-coordinates with the Cartesian velocity components, i.e.,

$$(\rho u)_x + (\rho v)_y = 0 \tag{3}$$

$$(\rho U)_\xi + (\rho V)_\eta = 0 \tag{4}$$

where the subscripts ξ and η denote the partial derivatives along the curvilinear coordinate lines. With regard to the covariant velocity components, defined as $\tilde{U}$ and $\tilde{V}$ here, i.e.,

$$\tilde{U} = x_\xi u + y_\xi v \tag{5}$$

$$\tilde{V} = x_\eta u + y_\eta v \tag{6}$$

the continuity equation written in the covariant velocity components is

$$(\rho\alpha_1\tilde{U} + \rho\beta_1\tilde{V})_\xi + (\rho\alpha_2\tilde{U} + \rho\beta_2\tilde{V})_\eta = 0 \tag{7}$$

where

$$\alpha_1 = \frac{q_{11}\, q_{22}^2}{J} \tag{8a}$$

$$\beta_1 = \alpha_1 \,(\vec{e}_\xi \cdot \vec{e}_\eta) \tag{8b}$$

$$\alpha_2 = \frac{q_{11}^2\, q_{22}}{J} \tag{8c}$$

$$\beta_2 = \alpha_2 \,(\vec{e}_\xi \cdot \vec{e}_\eta) \tag{8d}$$

$$q_{11} = (x_\xi^2 + y_\xi^2)^{1/2} \tag{8e}$$

$$q_{22} = (x_\eta^2 + y_\eta^2)^{1/2} \tag{8f}$$

$$J = x_\xi y_\eta - x_\eta y_\xi \tag{8g}$$

$\vec{e}_\xi$ and $\vec{e}_\eta$ are unit vectors along ξ- and η-directions, respectively, i.e.,

$$\vec{e}_\xi = \frac{x_\xi \vec{e}_X + y_\xi \vec{e}_Y}{q_{11}} \tag{9}$$

$$\vec{e}_\eta = \frac{x_\eta \vec{e}_X + y_\eta \vec{e}_Y}{q_{22}} \tag{10}$$

PHYSICAL AND GEOMETRIC CONSERVATION LAWS

When considering the various possible choices of velocity variables, one of the primary criteria is that in the framework of finite-volume formulation, a fully conservation-law form of governing equations is usually more desirable since it can satisfy the physical laws more easily and accurately. This consideration has a particularly important implication on the convection terms of the momentum equations since they are nonlinear and are usually a major source of numerical difficulty. With the Cartesian coordinates, the convection terms in momentum equations are of the form of $(\rho uu)_X + (\rho vu)_Y$, which is fully conservative. In a curvilinear coordinate system, these terms can be transformed in a straight forward manner with the use of the Cartesian velocity components as the primary dependent variables to the form of $(\rho Uu)_\xi + (\rho Vu)_\eta$ which is also fully conservative.

However, when either the contravariant or the covariant velocity components are used as the primary dependent variables, the fully conservative form can no longer be guaranteed since the linear momentum is conserved along a straight line, not a curved line. Thus the differential equations for both the contravariant and the covariant velocity components involve the source terms arising from the curvature of the coordinate lines. Furthermore, in the numerical implementation, the contravariant components ρU and ρV on each boundary of the mesh are defined as the mass flux between the two end points of the mesh boundary [7] and their values can artificially change with different grid systems. Hence, for the same flowfield the values of those contravariant and covariant velocity components can be greatly affected by the ways that the grid systems are generated. These aspects can cause difficulties in preserving high degrees of numerical accuracy in satisfying the conservation laws.

To demonstrate this point, consider the purely convective equation

$$(\rho uu)_X + (\rho vu)_Y = 0 \tag{11}$$

One of the most basic tests of the numerical accuracy of any computational algorithm for Eq. (11) can be made by generating a grid system with arbitrary skewness and nonuniformity and then to use this grid system to check the numerical accuracy of it by solving a uniform flow field of, say, ρ=1, u=1, and v=1. With this condition, Eq. (11) is trivially satisfied in the differential sense. Hence it serves as a good case to test whether an algorithm can honor the geometric aspect of the conservation laws in a discrete form. Here we call this

requirement the geometric conservation law [8] since the governing equations retain the conservation-law form but contain only the geometric quantities. The transformed equation of Eq. (11) with the Cartesian velocity components as dependent variables in curvilinear coordinates then becomes

$$(\rho Uu)_\xi + (\rho Vu)_\eta = 0 \tag{12}$$

which with the uniform flowfield is reduced to

$$(y_\eta - x_\eta)_\xi + (-y_\xi + x_\xi)_\eta = 0 \tag{13}$$

Referring to Fig. 1, Eq. (13) is discretized as follows:

$$(y_\eta - x_\eta)_e - (y_\eta - x_\eta)_w + (-y_\xi + x_\xi)_n - (-y_\xi + x_\xi)_s = 0 \tag{14}$$

where e, w, n and s denote the east-, west-, north-, and south-face of the mesh, respectively. If a consistent finite-volume formulation is adopted, as shown in [7], by approximating the derivative of the metric terms in Eq. (14) with the difference between two end points of the mesh line, then Eq. (14) becomes

$$\begin{aligned} &[(y_{i+1,j+1} - y_{i+1,j}) - (x_{i+1,j+1} - x_{i+1,j})] \\ &- [(y_{i,j+1} - y_{i,j}) - (x_{i,j+1} - x_{i,j})] \\ &+ [-(y_{i+1,j+1} - y_{i,j+1}) + (x_{i+1,j+1} - x_{i,j+1})] \\ &- [-(y_{i+1,j} - y_{i,j}) + (x_{i+1,j} - x_{i,j})] = 0 \end{aligned} \tag{15}$$

which is satisfied <u>exactly</u>, regardless of how skew or nonuniform the meshes are. It is also noted that one of the merits of this test problem is that since the flowfield is uniform, the whole focal point is directed toward the satisfaction of geometric requirements; other issues such as the appropriate approximation of the convection effects do not arise here.

Since our primary interest is for Navier-Stokes flow computation, it is useful to point out that the above geometric conservation law is applicable to the pressure gradient terms as well. However, the same requirements cannot be rigorously satisfied by the viscous terms (for flowfields of constant velocity gradients) due to the appearance of the nonlinear metric products associated with the coordinate transformation of the second-order derivative terms. Overall, one can summarize the situation by stating that with the use of Cartesian velocity components, the Navier-Stokes equations can be written in the strong conservation-law form in the curvilinear coordinate system. In terms of numerically satisfying the geometric conservation law, the first order derivatives, including the convection and pressure terms, can always achieve it. The degree of satisfaction of the viscous terms, on the other hand, is dependent upon the actual grid distribution.

For the use of curvilinear components, say, the contravariant vector, the equation corresponding to Eq. (11) can be obtained by performing a chain-rule type of coordinate transformation,

$$\left[\rho U^2/q_{11} \right]_\xi + \left\{ \begin{matrix} 1 \\ 1\ 1 \end{matrix} \right\} \rho U^2/q_{11} + \left\{ \begin{matrix} 1 \\ 1\ 2 \end{matrix} \right\} \rho UV/q_{11}$$

$$+ (q_{11}/q_{22}) \left[\rho UV/q_{11} \right]_\eta + \left\{ \begin{matrix} 1 \\ 1\ 2 \end{matrix} \right\} \rho UV/q_{22} + \left\{ \begin{matrix} 1 \\ 2\ 2 \end{matrix} \right\} \rho V^2 q_{11}/(q_{22})^2$$

$$- (\rho U/q_{11})U_\xi - (\rho U/q_{22})V_\eta = 0 \qquad (16)$$

where the Christoffel symbols of the second kind are defined as

$$\left\{ \begin{matrix} 1 \\ 1\ 1 \end{matrix} \right\} = \frac{y_\eta x_{\xi\xi} - x_\eta y_{\xi\xi}}{J} \qquad (17a)$$

$$\left\{ \begin{matrix} 1 \\ 1\ 2 \end{matrix} \right\} = \frac{y_\eta x_{\xi\eta} - x_\eta y_{\xi\eta}}{J} \qquad (17b)$$

$$\left\{ \begin{matrix} 1 \\ 2\ 2 \end{matrix} \right\} = \frac{y_\eta x_{\eta\eta} - x_\eta y_{\eta\eta}}{J} \qquad (17c)$$

It is now obvious that Eq. (16) not only possesses more terms than Eq. (11), but more critically it contains source terms resulting from the curvature of the coordinate line. Hence, it is no longer of the fully conservative form which can cause difficulties with the finite-volume formulation, especially if the grid system contains substantial nonuniformity and skewness. The fact that q_{11} and q_{22} are nonlinear with respect to the metric terms resulting from the coordinate transformation further compounds the difficulty of exactly satisfying the conservation law in a discrete manner. Similar case can be made to the equation cast in terms of the covariant velocity components.

The other observation related to satisfaction of the geometric conservation law can be made by studying the continuity equation written in terms of the covariant velocity components. Equation (7) demonstrates that the conservation law can be preserved in differential form for the covariant velocity components. However, because the terms α and β involve nonlinear combinations of metric terms, the geometric conservation law cannot be always honored in a skewed mesh system. It is clear that since the physical conservation laws are the ones that we ultimately strive to satisfy, the numerical algorithms not only preferably should be written to satisfy the strong conservation law in differential form, but also should satisfy the geometric conservation law in discrete manners. The latter requirement cannot be satisfied as long as the equations contain nonlinear metric terms regardless of whether the fully conservation

law form is adopted in the differential equations or not.

In summary, it has been demonstrated here that with either the contravariant and covariant velocity vectors, the momentum equations in curvilinear velocity vectors are no longer of full conservation-law forms. The curvatures of the grid lines introduce extra source terms into the governing equations which cause the degrees of satisfaction of physical conservation laws sensitive to the uniformity and skewness of the mesh distribution. For the continuity equation, on the other hand, the contravariant velocity can maintain both the fully conservative form and compactness of the equation. Table I summarizes the points discussed above. It appears that a combined use of the contravariant velocity components, for the continuity equation, and the Cartesian velocity components, for momentum equations, is a good balance [7,9]. This practice has particular merits in a pressure-correction type of algorithm where the velocity corrections are derived based on the information of pressure correction. As discussed in [9], the contravariant components should be used in the velocity-correction procedure to ensure the satisfaction of the conservation laws.

Table I. Choice of Primary velocity variables versus satisfying physical and geometric conservation-law forms for momentum and continuity equations

	Momentum Equations			
	Convection	Pressure	Viscous	Continuity Equation
Cartesian	satisfies both physical and geometric laws	satisfies both physical and geometric laws	satisfies physical but not geometric laws	satisfies both pysical and geometric laws
Contravar-iant	does not satisfy either law	satisfies both laws	does not satisfy either law	satisfies both laws
Covariant	does not satisfy either law	satisfies both laws	does not satisfy either law	satisfies physical but not geometric law

GRID SYSTEM

In [7,9], a staggered grid system has also been, adopted. As shown in Fig. 1, the Cartesian and contravariant velocity components are defined at the middle of east-west and north-south faces, respectively. That is, in 2-D curvilinear coordinates designated as ξ-lines and η-lines, u and U components are defined at the middle of η-lines of the mesh, and v and V components are defined at the middle of ξ-lines of the mesh. All the scalar variables including pressure, temperature, and density are located at the geometric center of the four vertices defining the mesh. References [4-6] suggest that with the combined use of the Cartesian velocity components and the staggered grid arrangement, difficulties arise when the grid lines turn ninety degrees from the original orientations, and the benefits of the grid staggering are lost.

A detailed discussion has been given in this regard in Ref. [3]. It was demonstrated that, if the metric terms between (x,y) and (ξ,η) coordinates are nonconstant, then the spurious pressure oscillations do not appear in both the staggered and nonstaggered grid. For the staggered grids, moreover, the problem of spurious pressure oscillations can be prevented even with the constant metric terms. One can simply define the curvilinear coordinates to be non-parallel to the Cartesian coordinates. Afterall, there is no reason to always insist on defining the ξ-lines in the inlet region to be parallel to x-lines.

Besides the algorithms utilizing the staggered grid arrangement, methods based on the nonstaggered grid arrangement have also been proposed for both the pressure and density-based algorithms, e.g., [10,11]. These methods require special procedures to prevent the decoupling of the velocity and pressure fields from exhibiting the chequerboard oscillations. For example, in [10] an explicit fourth-order pressure dissipation term is added to the pressure correction equation to suppress the spurious oscillations. However, with the use of finite mesh sizes, in reality the artificially added fourth-order gradient term may not be smaller than the original lower order derivative terms especially when there are large gradients present in the flowfield, as demonstrated by a Fourier type of analysis [12]. Hence the actual degrees of numerical accuracy may be affected by the numerical smoothing procedure. Furthermore, it is also well known [1] that artificially generated boundary conditions are needed for the pressure in a nonstaggered grid system. With the use of the staggered grid system, there is no need to devise artificial boundary conditions for the pressure correction equation [7] regardless of the orientation of the coordinate system. In terms of the momentum equations, since in general both P_ξ and P_η terms appear in both u- and v- momentum equations, some extrapolation procedures will still be needed for both types of grid arrangement. Table II summarizes the need of prescribing pressure boundary conditions in staggered and nonstaggered grid systems.

Table II. Grid systems versus need of pressure boundary conditions

	u-momentum equation	v-momentum equation	Continuity (or pressure) equation
Staggered Grid	needs artificial condition for p_η only	needs artificial condition for p_ξ only	needs no artificial condition
Non-staggered Grid	needs artificial conditions for both p_ξ and p_η	needs artificial conditions for both p_ξ and p_η	needs artificial condition

PRACTICAL FLOW EXAMPLES

Several examples of direct relevance to the aforementioned issues are presented. Results of flows in domains with ninety-degree and three-hundred-sixty-degree turnings are shown here. The first example shown is a diffuser with 90-degree turning (called a draft tube) which, as shown schematically in Fig. 3, has a fivefold increase of cross-sectional area from the inlet to the outlet. The shape of cross-section also varies from circular at inlet to rectangular at outlet. For this flow device, the static pressure recovery factor depends greatly on the inlet flow conditions imposed by the turbine runner exit velocity profiles. A series of theory/data comparisons has been conducted under different operating conditions [14,15]. Selected results of turbulent flow cases with $Re=10^6$ will be presented here. The numerical solutions were obtained by using the standard k-ϵ two-equation turbulence closure. Four grid sizes, with 7x11x13, 11x15x45, 18x21x61 and 21x29x81 nodes, have been adopted to assess numerical accuracy with respect to spatial resolution. The convection terms in the momentum equations were approximated by the second-order upward scheme. Both viscous and pressure terms were approximated by the standard central difference schemes.

Figures 2a and 2b show direct photographic information of two different operating conditions, full load and partial load. Figure 3a illustrates a 3-D view of the draft tube flow characteristics at full load condition. The velocity vectors are shown at the inlet and outlet sections. All the solid lines starting at the center region of the inlet section and finishing at the outlet section represent the streaklines of the mean velocity flow field. The twisted streaklines starting at the draft tube inlet center simulate correctly the straight rope observed at full load condition as shown in Figure 2a. The typical contra-rotating (opposite to the runner direction) free vortex flow at the draft tube inlet is shown in Figure 3b. The display of the velocity vectors in the main stream direction at the mid-section is represented in Figure 3c. The very weak velocity core, observed at the middle of the conical section, also indicates the

presence of a rope at the center.

Figures 4a to 4c illustrate the draft tube behavior at partial load condition with a very high co-rotating inlet swirl. The display of the velocity vectors in the main stream direction at the mid-section indicates that a large flow recirculation zone is taking place in the conical section. The twisted spiral streaklines starting from the draft tube inlet center are very similar to the spiral rope observed in the laboratory flow visualization as shown in Figure 2b.

In order to study the evolution of the static and dynamic pressures along the main flow direction, massflow-weighted average values of these properties at each cross section are calculated. The numerical results are then compared with the experimental data in Figure 5. At the ordinate, the pressures are normalized by the inlet dynamic pressure. At the abscissa the center line length is normalized by the draft tube inlet diameter. Results from the two finer grid systems predict very well the variation of all the pressures, specially in the accelerating region located at the end of the elbow section. The agreements between prediction and measurement worsen as grid resolutions degrade.

The flow behavior in the elbow draft tube, with an optimal inlet swirling flow, was investigated in detail with pitot traverses taken from several cross sections. The experimental data are compared with numerical results. The display of the velocity vectors in the main flow direction is shown in Figure 6. The numerical result obtained with the 18x21x61 grid system is presented. Observation of the velocity vector distribution at different elevation and plan views indicates clearly that a large recirculation zone occurs at the middle of the elbow section. Further downstream, flow separation appears at the center and near the top of the draft tube. Also toward the outlet of the draft tube, the flow is somewhat shifted to one side wall. This tendency is more accentuated with a stronger inlet swirling flow. The comparison of the predicted head losses with experimental data is shown in Figure 7. The head loss is about 2% for optimal load, but it increases rapidly for off-design conditions. The numerical result agrees very well with laboratory measurement for the whole range of the runner operating conditions, except for very high swirl intensity at partial load where flow instability was observed during the test.

The next example is also a 90-degree turning duct but with neither area changes nor cross-sectional shape variations. Figure 8 shows some schematic illustration of the geometry, grid distribution, and velocity as well as static pressure solution. Figure 9 shows the static pressure distribution along the center line of the outer and inner walls. Same as the previous examples, no oscillation of pressure field are observed.

As a further demonstration, a flow domain of 360-degree turning, the so-called casing, is used. The schematic representations of the casing, including the overall geometry, the evolution of the size of cross-section, and representative grid distributions are summarized in Fig. 10. The fluid enters from the upstream inlet and exits through the inner circumferencial surface. The grid system is of the size of 95x21x13 nodes. Figure 11 shows a top-view of a casing with smooth

and continuous turning. Figure 12 shows the computed particle trajectories in short time durations and static pressure distributions in the middle top-view plane for a laminar flow. The Reynolds number based on the fluid kinematic viscosity, the incoming uniform velocity and the inlet diameter of the present case is 100. It can be seen that throughout the whole flow domain, no spurious oscillations are present in numerical solution. With the given Reynolds number, the flow in the casing shows combined characteristics of that through a pipe (in the outer portion of the casing) and that into a sink (in the inner portion of the casing). Figure 13 shows a turbulent flow calculation with $Re=10^6$ and with the standard $k-\epsilon$ model. For the high Reynolds number flow, there is less influence of the mean pressure gradient along the circumferential direction than along the radial direction. Again, no spurious oscillations are present in Fig. 13.

CONCLUSIONS

The present work aims at investigating the fundamental issues of adopting the velocity variables and grid systems for computing the complex fluid flow in irregular geometries with the employment of a non-orthogonal curvilinear coordinate system. It is clear that the strong conservation-law in differential forms can be completely retained by the use of Cartesian velocity components. However, the use of the covariant or contravariant velocity components generally introduces source terms into the differential governing equations due to the curvature effects. In the framework of the finite-volume approach, the momentum equations based on the Cartesian velocity components can satisfy the geometric conservation law for both convection and pressure terms. The second derivative (viscous) terms involve nonlinear metric terms and hence do not guarantee the satisfaction of the geometric conservation law. For the equations based on the curvilinear velocity components, the nonlinear metric terms appear in both the first and second derivative terms. Coupled with the curvature source terms, the utilization of the curvilinear velocity components as the primary variables makes the degree of satisfaction in terms of honoring the geometric conservation law more influenced by the grid skewness. A unique issue facing the use of the Cartesian velocity components along with a staggered grid arrangement is that of a 90-degree turning. It is demonstrated here that satisfactory solutions can be obtained with this approach even with the 90-degree and 360-degree turnings.

REFERENCES

1. Peyret, R. and Taylor, T. D., Computational Methods for Fluid Flow, Springer-Verlag, New York (1983).

2. Correa, S. M. and Shyy, W., "Computational Models and Methods for Continuous Gaseous Turbulent Combustion," Prog. Energy Combust. Sci., 13, 249-292 (1987).

3. Shyy, W. and Vu, T. C., "On the Adoption of Velocity Variable and Grid System for Fluid Flow Computation in Curvilinear Coordinates," accepted for publication in J. Comput. Phys..

4. Yang, H. Q. and Yang, K. T., "Buoyant Flow Calculations with Non-Orthogonal Curvilinear Coordinates for Vertical and Horizontal Parallelpiped Enclosures," Inter. J. Numer. Meths. Engrg., 25, 331-345 (1988).

5. Karki, K. C. and Patankar, S. V., "Calculation Procedure for Viscous Incompressible Flows in Complex Geometries," Numer. Heat Transf., 14, 295-307 (1988).

6. Wittig, S., Bayer, H. J. and Noll, B., "On the Application of Finite-Difference Techniques for the Computation of the Flow Field in Gas Turbine Combustors with Complex Geometries," in Combustion and Fuels in Gas Turbine Engines, AGARD CP No. 422, Paper No. 28 (1988).

7. Shyy, W., Tong, S.-S. and Correa, S. M., "Numerical Recirculating Flow Calculation Using a Body-fitted Coordinate System," Numer. Heat Transf., 8, 99-131 (1985).

8. Thomas, P. D. and Lombard, C. K., "Geometric Conservation Law and Its Application to Flow Computations on Moving Grids," AIAA J., 17, 1030-1037 (1979).

9. Braaten, M. E. and Shyy, W., "A Study of Recirculating Flow Computation Using Body-fitted Coordinates: Consistency Aspects and Mesh Skewness," Numer. Heat Transf., 9, 559-574 (1986).

10. Rhie, C. M., "A Pressure Based Navier-Stokes Solver Using the Multigrid Method," AIAA Paper No. 86-0207 (1986).

11. Kwak, D. K., Chang, J. L. C., Shanks, S. P. and Chakravarthy, S. R., "An Incompressible Navier-Stokes Flow Solves in Three-Dimensional Curvilinear Coordinate System Using Primitive Variables," AIAA Paper NO. 84-0253 (1984).

12. Shyy, W., "A Study of Finite Difference Approximations to Steady-State Convection-Dominated Flow Problems," J. Comput. Phys., 57, 415-438 (1985).

13. Vu, T. C. and Shyy, W., "Viscous Flow Analysis as a Design Tool for Hydraulic Turbine Components," ASME J. Fluids Engrg., (to appear).

14. Vu, T. C. and Shyy, W., "Viscous Flow Analysis for Hydraulic Turbine Draft Tubes," ASME J. Fluids Engrg., (to appear).

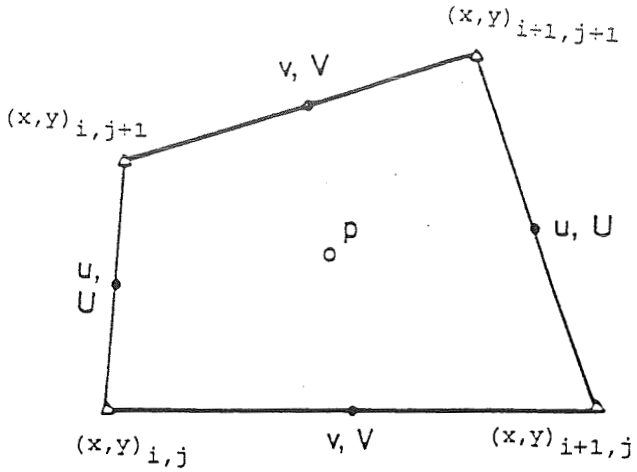

Fig. 1 Configuration of a staggered grid system.

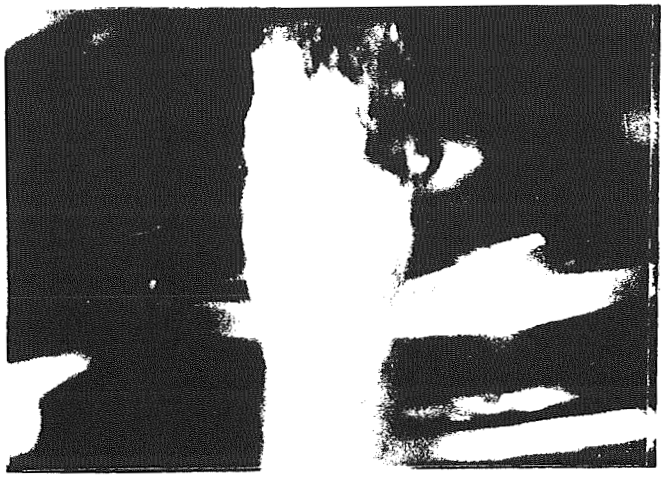

Fig. 2a Francis runner exit flow characteristics at full load condition.

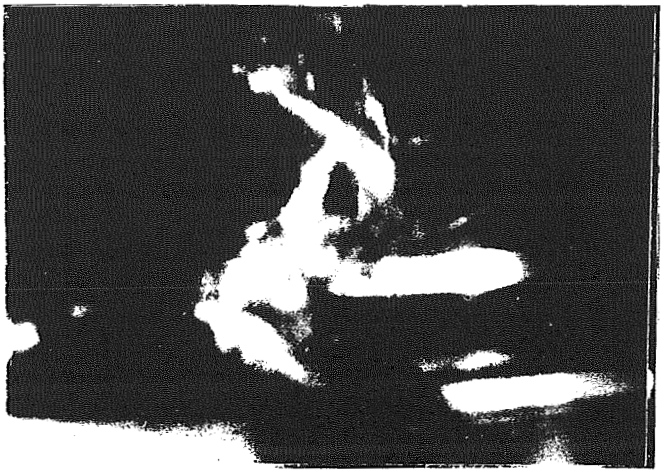

Fig. 2b Francis runner exit flow characteristics at partial load condition.

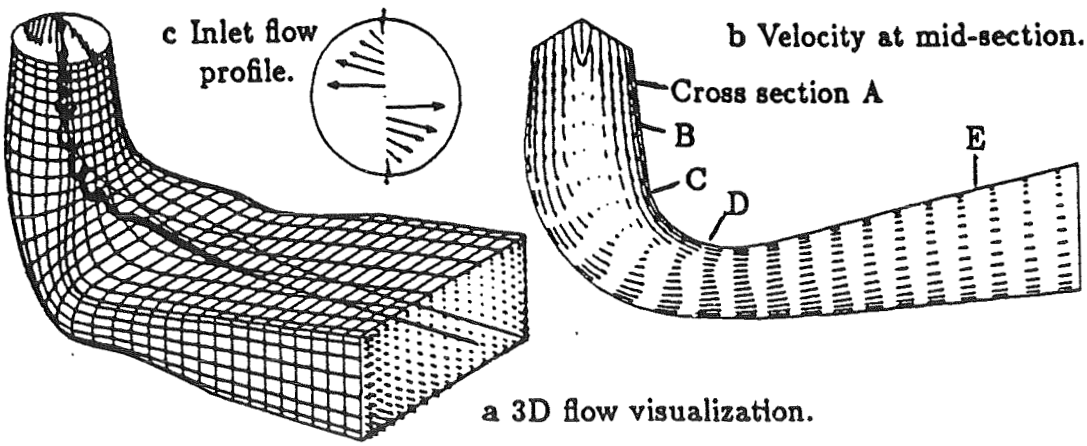

Fig. 3 Draft tube flow characteristics at full load condition.

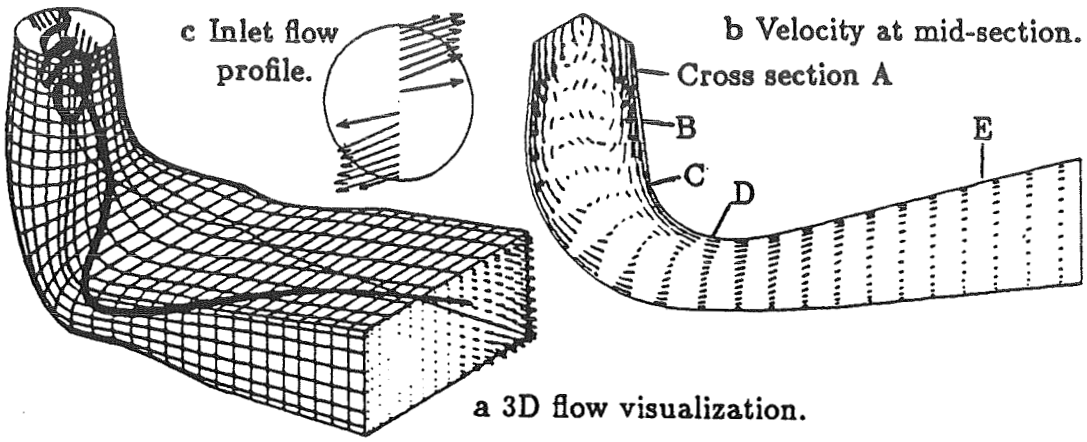

Fig. 4 Draft tube flow characteristics at partial load condition.

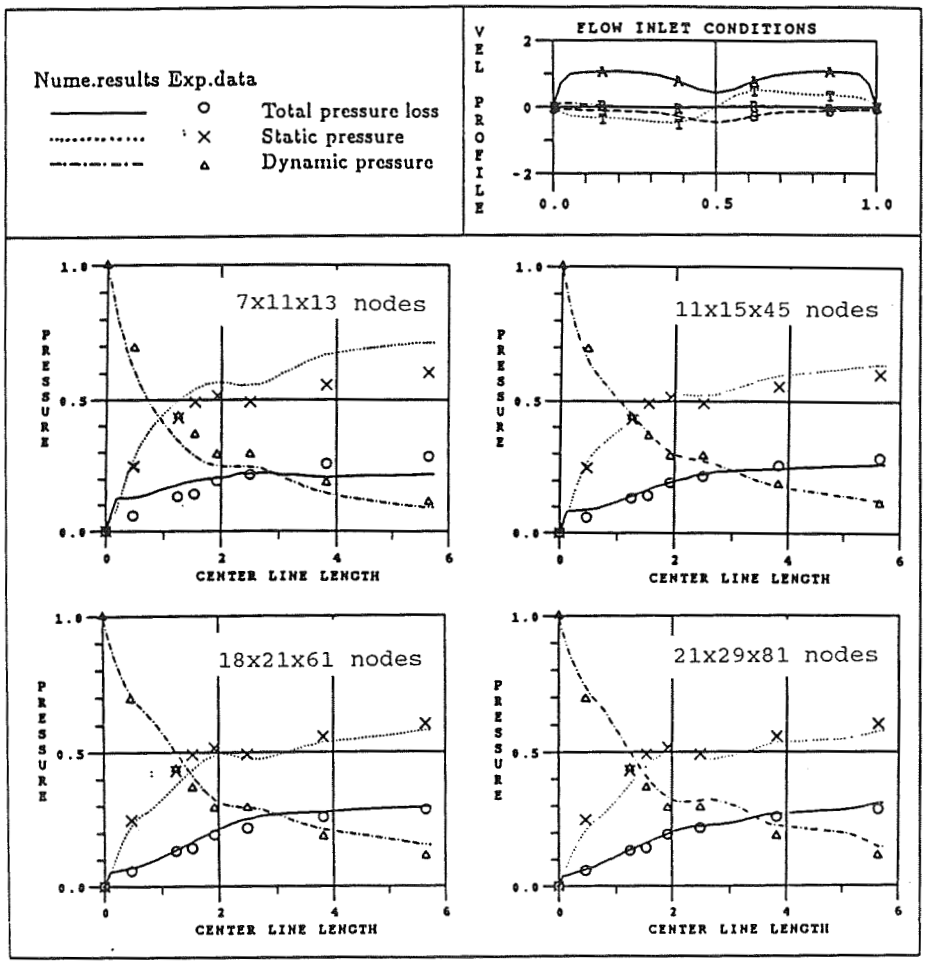

Fig. 5 Flow behavior with inlet swirling flow. Evolution of dynamic and static pressure and of total pressure loss.

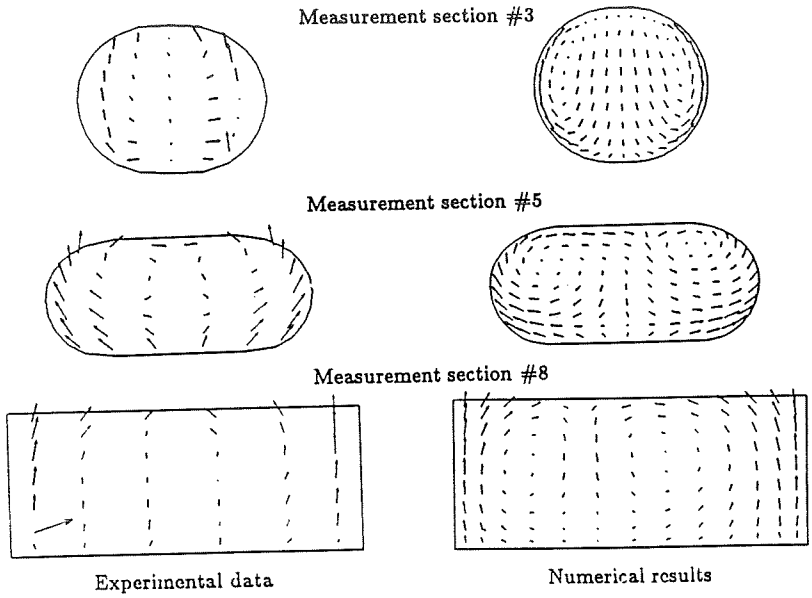

Fig. 6 Flow behavior with inlet uniform flow - Secondary flow (Flow coming toward the reader).

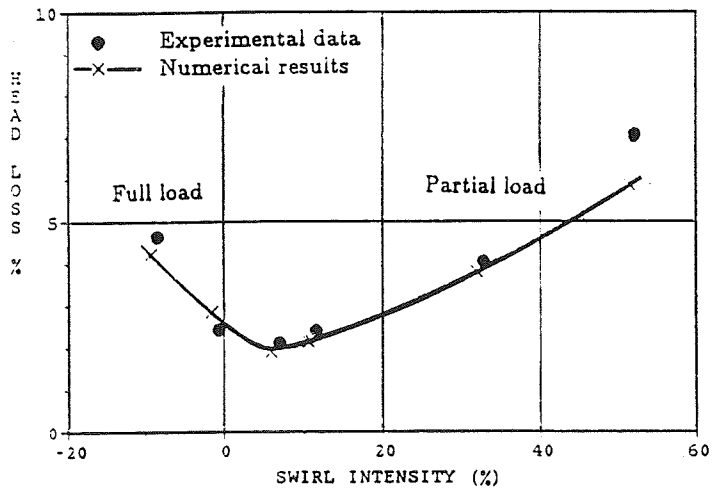

Fig. 7 Head losses in an elbow draft tube for different turbine operating conditions. Comparison between numerical results and experimental data.

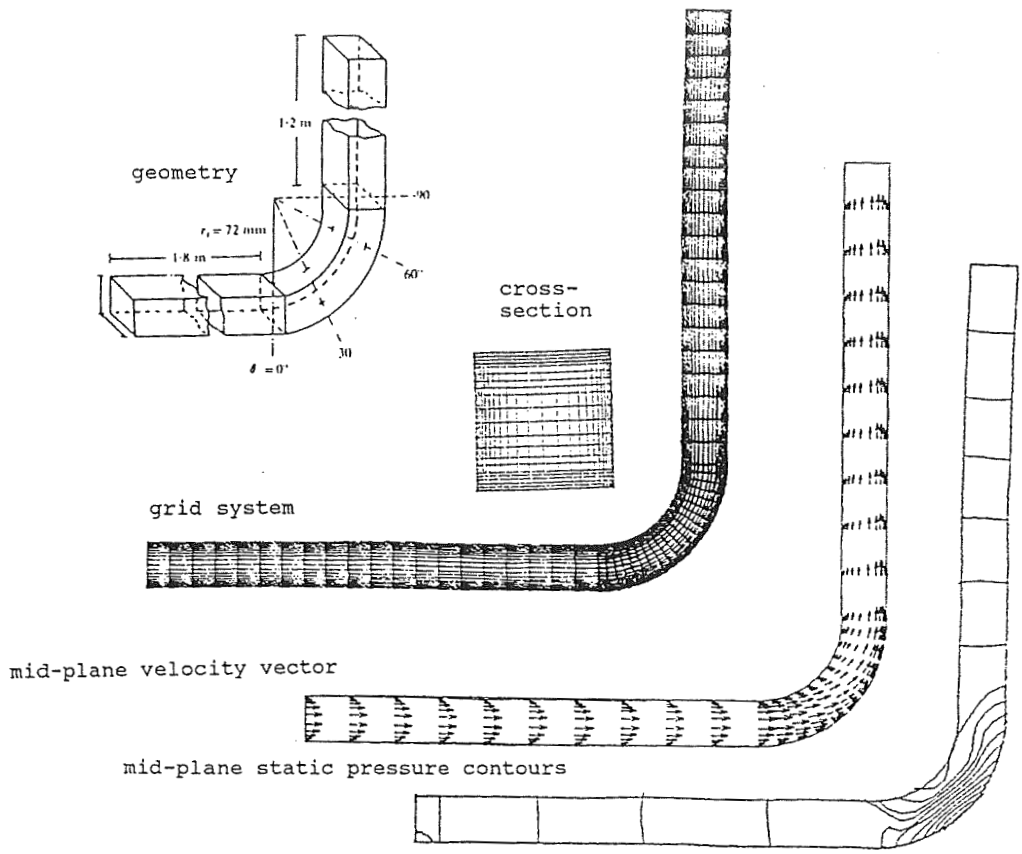

Fig. 8 Geometry, grid, velocity, and pressure of a 90-degree turning duct of constant cross-section.

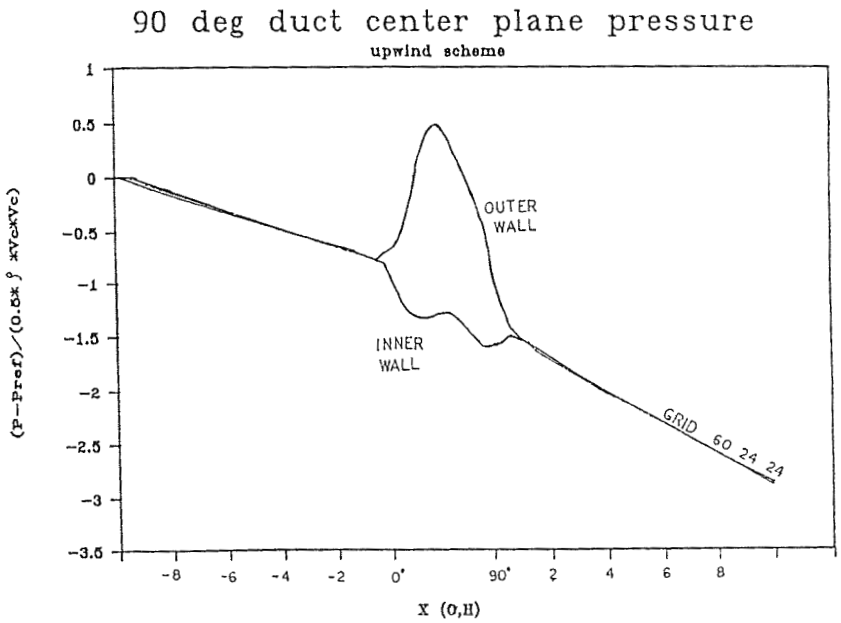

Fig. 9 Static pressure along center line of 90-degree turning duct with constant cross-section.

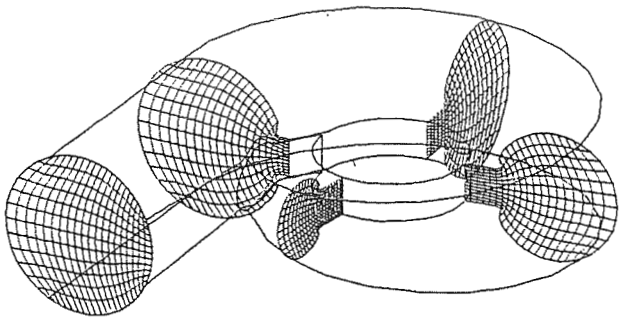

Selection grid distribution in cross-sectional planes

Fig. 10 Geometry and grid system of casing with 360-degree turning.

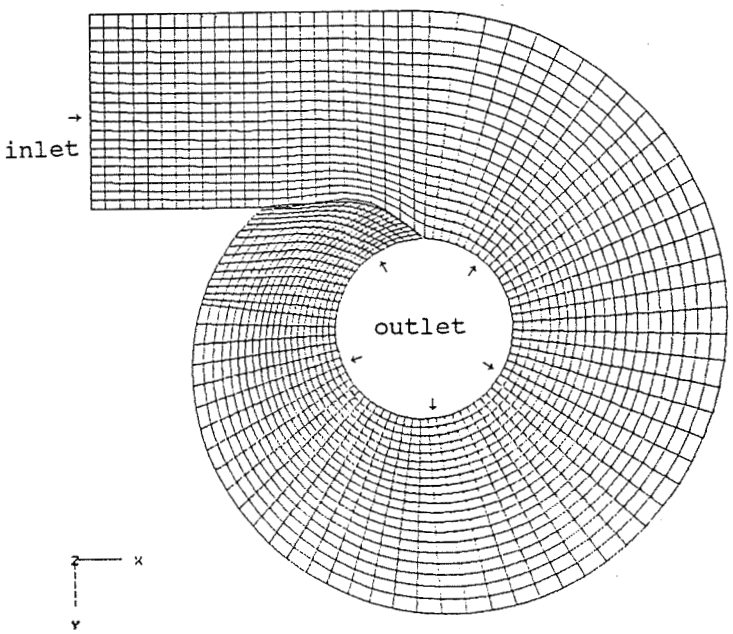

Fig. 11 Grid system in top-view plane of a casing with smoothly varying wall contours.

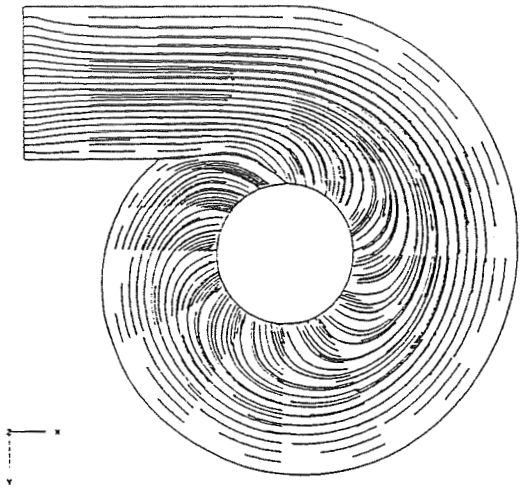

particle trajectories

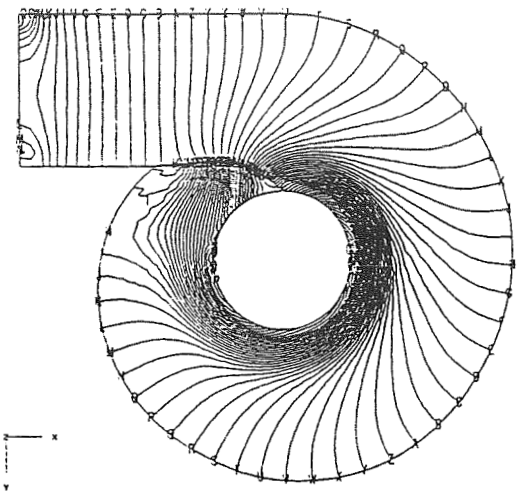

static pressure contours

Fig. 12 Solution of laminar flow (Re=100) in a casing with smoothly varying wall contours.

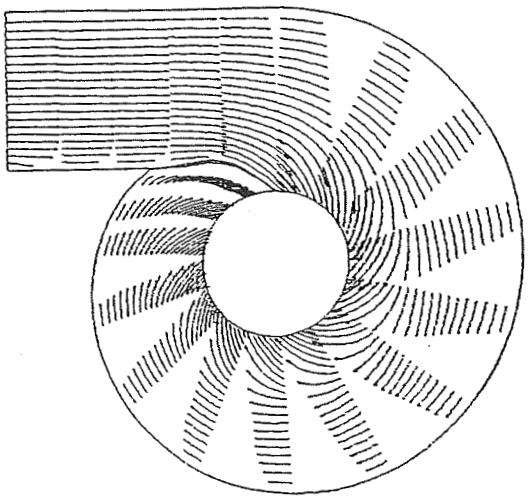

particle trajectories

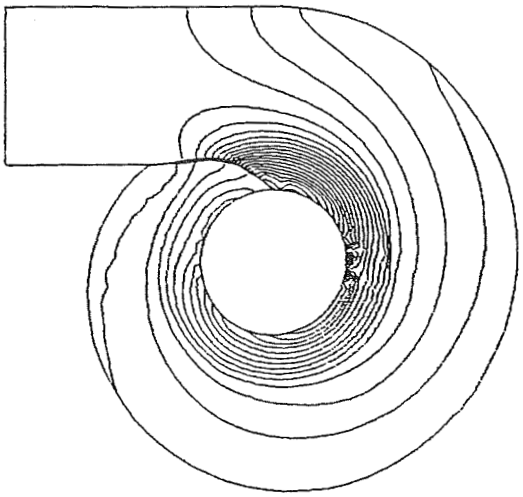

static pressure contours

Fig. 13 Solution of turbulent flow ($Re=10^6$) in a casing with smoothly varying wall contours.